

Crustal and upper-mantle structure in the Eastern Mediterranean from the analysis of surface wave dispersion curves

F. Di Luccio¹ and M. E. Pasyanos²

¹*Istituto Nazionale di Geofisica e Vulcanologia, via di Vigna Murata 605, 00143, Rome, Italy;*
diluccio@ingv.it

²*Earth Science Division, Lawrence Livermore National Laboratory, Livermore, California, USA;*
pasyanos1@llnl.gov

Geophys. J. Int., Accepted 2006 December 12. Received 2006 December 11; in original form 2006 July 4

SUMMARY

The dispersive properties of surface waves are used to infer earth structure in the Eastern Mediterranean region. Using group velocity maps for Rayleigh and Love waves from 7-100 s, we invert for the best 1D crust and upper-mantle structure at a regular series of points. Assembling the results produces a 3D lithospheric model, along with corresponding maps of sediment and crustal thickness. A comparison of our results to other studies finds the uncertainties of the Moho estimates to be about 5 km. We find thick sediments beneath most of the Eastern Mediterranean basin, in the Hellenic subduction zone and the Cyprus arc. The Ionian Sea is more characteristic of oceanic crust than the rest of the Eastern Mediterranean region as demonstrated in particular by the crustal thickness. We also find significant crustal thinning in the Aegean Sea portion of the back-arc, particularly towards the south. Notably slower S-wave velocities are found in the upper-mantle, especially in the northern Red Sea and Dead Sea Rift, central Turkey, and along the subduction zone. The low velocities in the upper-mantle that span from North Africa to Crete, in the Libyan Sea, might be an indication of serpentinized mantle from the subducting African lithosphere. We also find evidence of a strong reverse correlation between sediment and crustal thickness which, while previously demonstrated for extensional regions, also seems applicable for this convergence zone.

Key words: surface waves, Eastern Mediterranean, lithosphere, Moho depth

INTRODUCTION

The eastern Mediterranean basin (Fig. 1) is tectonically complex and its evolution is strongly related to the active subduction along the Hellenic arc. The present tectonics are driven by the collision of the African and Eurasian plates, the Arabian-Eurasian convergence and the displacement of the Anatolian-Aegean microplate. The boundary between the African and the Anatolian-Aegean microplates is delineated by the Hellenic arc, the Pliny-Strabo trench, the Florence Rise and Cyprus in the west, while in the east the boundary has been identified in the Herodotus basin or east of Cyprus (Aksu *et al.*, 2005 and references therein). The Cyprian and Hellenic arcs are dominated by compression, whereas to the east of Cyprus a left-lateral motion with an eastward increasing of the tensional component (near the DSF) is predominant.

Plate motion slip rates have been accurately determined by recent GPS data (McClusky *et al.*, 2000 and 2003); a slip rate of ~6 mm/yr is associated to the northeastward motion of the African plate whereas the northward motion of the Arabian plate has rate of ~18 mm/yr. The differential motion of Africa and Arabia relative to Eurasia is accommodated by the sinistral transpressional Dead Sea Transform Fault (DSF). Northward motion of the Arabian plate relative to Eurasia causes crustal shortening and thickening in Eastern Turkey.

The timing and the origin of the extension in the Aegean is not yet established. Two main hypothesis have been proposed: the extension occurs in the back arc basin of the Hellenic subduction zone or it is older than the opening of the back arc basin and is due to gravitational collapse of thick

crust. Although a unique explanation is not yet given, it is globally accepted that the combination of the subduction system to the west and the convergence of the plates to the east produces the westward motion of the Anatolian microplate, which is bounded by strike-slip faults, the dextral North Anatolian Fault (NAF) to the north and the left-lateral East Anatolian Fault Zone (EAF) to the south-east. McClusky *et al.* (2000 and 2003) find that the rate of motion along the Hellenic trench reaches its maximum (~35 mm/yr) within the Gulf of Corinth and central Greece. Lateral motion along the NAF is ~24 mm/yr, with a slight compression along the eastern segment and extension in the Marmara Sea-North Aegean Trough. A slip rate of 9 mm/yr along the EAF is derived, while along the DSF left-lateral transpressive motion at ~6 mm/yr is found in the north and pure left-lateral strike-slip at 5.6 mm/yr is derived in the south (McClusky *et al.*, 2000 and 2003).

The distribution of seismicity as shown in Figure 1 is mainly concentrated along the Hellenic trench, Greece and Aegean region, along the NAF and EAF and the Cyprian arc, with deeper earthquakes occurring along the subduction zones (black dots in the Tyrrhenian Sea and along the Hellenic arc). The seismicity of Cyprus is distributed differently along the arc; the eastern segment is the locus of shallow and intermediate earthquakes whose magnitude can be larger than 6, whereas the western portion contains deep and low magnitude events. The seismicity of the Hellenic trench is in contrast distributed regularly along the arc with hypocentral depths extending down to 300 km. The difference in the seismicity trend along the two arcs confirms the dissimilar plate motion in the two regions. Subduction is active beneath the whole length of the Hellenic trench whereas the Cyprian arc is undergoing subduction along its northwestern margin, collision in the south-eastern part and

transcurrence along its eastern segment (Wdowinski *et al.*, 2006).

The determination of crustal thickness has been the purpose of many published works in which a variety of geophysical techniques have been applied. Recent receiver function, surface wave, gravity data inversion, and tomographic studies (for example Li *et al.*, 2003; Marone *et al.*, 2003; van der Meijde *et al.*, 2003; Zor *et al.*, 2003; Endrun *et al.*, 2004; Hofstetter & Bock, 2004; Meier *et al.*, 2004; Tirel *et al.*, 2004; Al-Damegh *et al.*, 2005; Karagianni *et al.*, 2005; Koulakov *et al.*, 2005; Makris & Yegorova, 2005; Mohsen *et al.*, 2005; Zhu *et al.*, 2006) have derived the Moho depth and mapped shear-wave velocity in different sites in the Eastern Mediterranean region. Here, we wish to provide a more regional perspective on parameters such as crustal thickness, sediment thickness, crustal velocities, and upper-mantle velocity in order to address questions about the tectonics of the region.

Crustal thickness beneath the Eastern Mediterranean varies from oceanic to continental and the thickness of sediments plays an important role in determining the nature of the crust. For example, the nature of the crust in the Levantine basin, south of Cyprus and west of the Israel and Lebanon margins, has been defined as oceanic (Khair & Tsokas, 1999) or continental (Ben Avraham *et al.*, 2002). In the first case the Levantine basin formed by the rifting of African continental crust fragments, whereas in the latter case, a sediment layer of 14-15 km overlies a thinned Precambrian continental crust. In a recent study, Ritzmann *et al.* (2006) found a strong negative correlation between sediment thickness and the thickness of crystalline crust in the extensional tectonic regime of the Barents Sea. Where the crust has been extended (thin crust), there was a correspondingly thick sediment profile.

Although a large number of studies on the Eastern Mediterranean have been done, there are still a certain number of issues to be addressed such as the timing and the style of deformation of the basin, the nature and thickness of the crust. In this study we present new results of surface wave analysis for the lithospheric structure in the Eastern Mediterranean region. Our goal is to address questions like what type of crust (oceanic or continental) is beneath the Hellenic subduction system, how deep are the sediments in the Eastern Mediterranean region, and how do shear wave velocities vary in the lower crust and upper- mantle. In order to address these issues, we use the dispersion characteristics of the largest amplitude waves recorded in seismograms to determine structure velocity in the eastern Mediterranean region. The results presented here are relevant for defining the lithospheric structure of the eastern Mediterranean basin and its interaction with surrounding plates.

DATA AND METHODOLOGY

We invert for crust and upper-mantle structure using surface wave group velocities. Group velocities for the region were determined from the tomographic inversion of thousands of dispersion measurements from 40 years of seismic data. Dispersion curves were computed applying a multiple-filter analysis technique to the broadband displacement seismograms at different periods (Herrmann, 1973 and references therein). In addition to the large set of dispersion measurements from Pasyanos (2005), new group velocity measurements in the region have been made for this study. Stations in the region were gathered from a variety of sources (GSN, MEDNET, MIDSEA, PASSCAL, etc.) and included stations in Turkey (ANTO, ISP, MALT), Israel (BGIO, JER, KSDI, MRNI), Cyprus (CSS),

Greece (APER, IDI, ITHO, KOUM, SANT), Libya (GHAR, MARJ), and Jordan (RUW) in our study area. This provided us with excellent coverage of the region over a wide period range (Figure 2). Due to the poorer signal-to-noise ratio on the horizontal components, however, the number of Love wave measurements is generally less than the number of Rayleigh wave measurements.

We have tomographically inverted the measurements for regional group velocities using a variable-resolution inversion method and a grid size of $1^\circ \times 1^\circ$ (Pasyanos, 2005). The variable-resolution method employed in that study smooths the model significantly in poorly covered regions and only minimally smooths the model, allowing the highest resolution, in densely sampled regions like the eastern Mediterranean. We computed regional group velocity maps for Rayleigh and Love waves between 7 and 100 s, and the resulting maps are strongly correlated with structure. Figure 3a shows tomography results for the same periods shown in Figure 2 and the corresponding uncertainties are plotted in Figure 3b. At 15 seconds, the Mediterranean is clearly outlined by the slow velocities from the sediments in the basin. By 30 seconds, the slow velocities are limited to regions around Crete and Cyprus that have the thickest sediments. By 50 seconds, the kernels are sensitive to deeper structure and regions that have thick crust (like Central Anatolia) now appear slow.

Uncertainties in the tomographic model are computed using a bootstrapping method as described in Pasyanos & Walter (2002). Subsets of the dataset are formed and each of them is inverted with a randomized initial model, and the uncertainties are derived from the variations of the results. The resolution of the group velocities depends on data coverage, but is limited by the surface wave wavelength. Keeping in mind the good ray coverage of the region (Figure 2), at all but the shortest

periods (< 10 s), the resolution should be approaching the wavelength of the surface waves. This is less than 1° for periods shorter than 30 s, between 1 and 2° for 30 – 60 sec waves, and greater than 2° for periods longer than 60 s. Based on the sensitivity kernels of the surface waves, we should have very good resolution for shallow structure (sediments and crust), but at best have resolutions of 2° for deeper structure like the upper-mantle.

We derive the velocity structure from the tomographically-derived dispersion maps using a series of 1D inversions at each 1° point in the model. A linearized inversion method was used with a starting velocity model consisting of homogeneous horizontal layers (Herrmann & Ammon, 2002). As starting model we use CRUST2.0 (Bassin *et al.*, 2000) for the two sediment and the three crustal layers, and IASP91 (Kennett & Engdahl, 1991) to model the mantle velocity structure. The inversion procedure consists of taking the starting velocity model, calculating the predicted dispersion curve, and comparing it with the observed dispersion. The starting model is then iteratively refined until it fits the observations. Iterations are controlled to avoid artifacts like spurious low velocity zones. We alternatively invert for the layer thickness and layer velocity. The V_p/V_s ratio for each layer is fixed, while the density is derived from the P-wave velocity. Anisotropy has not included in this study, as we only inverted for isotropic structure. Each layer is equally weighted. The least squares inversion includes a damping factor that limits the size of model variations between each iteration. This limits overfitting the data with non-physical models. When the residual between the observed and predicted data remains constant, then the change in models corresponding to different iterations is negligible. The damping factor affects how fast the model converges and residuals between the observed and predicted

values are reduced. This reduces the likelihood of getting stuck in local minima.

Figure 4 is an example of the 1D inversion for a point in Israel (32°N – 35°E) where the group velocity fit for Rayleigh and Love waves is shown. In the same figure the comparison of the velocity model obtained from the inversion (dashed line) to the initial model (solid line) evidences the differences in the upper-mantle shear wave velocities and the crust thickness. Compared to our starting model, the surface waves require significantly slower upper-mantle velocities, thicker sedimentary layers and a deeper Moho. At the shortest periods (< 20 s) the Love waves are poorly fit. Love waves resolution for these periods is in general poorer than that of Rayleigh waves because of the smaller number of measurements and the lower signal to noise ratio, but this is reflected in the higher uncertainties of these dispersion values. In Figure 4, we also plotted the velocity model obtained from the inversion in which a unique starting model was used for all cells. The chosen velocity model (gray line) is IASP91 to which a thin sedimentary layer has been added to fit better the group velocity measurements at shorter periods. The resulting model (dashed gray line in the bottom panels of Figure 4) is similar to the one obtained using CRUST2.0+IASP91, although some discrepancy is observed in the crustal thickness. So, using two different velocity models as starting models, the uncertainties are in the range ± 5 km for the crustal thickness and ± 0.2 km/s in the shear wave velocity as shown in Pasyanos & Walter (2002).

CRUSTAL AND UPPER-MANTLE STRUCTURE: RESULTS

In Figure 5 we plot the thickness of sediment and crustal layers. We compare the results from this study with the initial thicknesses from CRUST2.0 overlaying IASP91. In a global overview final maps reflect the main features of the initial model but several and significant details are observed in our results. Thick sediments are found beneath the eastern Mediterranean basin, in particular soft sediments thicker than in the starting model. This is specifically true beneath southern Greece, northwestern Aegean Sea, southwest Turkey and Cyprus trench. However thinner soft sediments are found beneath the southwestern part of the Mediterranean basin. In the Levantine basin a sediment layer of 8-10 km is observed which is mostly composed of hard sediments (~6-7 km). A recent study (Netzeband *et al.*, 2006), based on refraction seismic data, has revealed a sedimentary layering roughly composed of ~4-5 km Plio-Quaternary material and evaporites and ~6-8 km of older (from Jurassic to Miocene) sediments in the Levantine basin. These two layers, if associated with the soft and hard sediment layers displayed in Figure 5, confirm that there is a good agreement with Netzeband *et al.* (2006). Indeed the thick sediments (~12 km) we have found in the Eratosthenes seamount do not match the results by Netzeband *et al.* (2006), although the sediment depth eastward is in agreement. In fact Netzeband *et al.* (2006) found that the sedimentary layer of 5 km beneath the seamount deepens to ~14 km beneath the basin to shallow again beneath the Dead Sea Fault. The same trend can be observed in Figure 5 along the same path.

In Figure 5 the crustal thicknesses are shown in the last three layers. Although characteristic

blocks are repeated in the final maps (right panels), important differences are revealed with respect to the initial model. The images in Figure 5 (right panels) evidence the thickening of the three crustal layers with respect to CRUST2.0+IASP91 (left panels). There is an overall increase in the crustal thickness, with the mid and lower crustal layers showing the most significant thickening. This crustal thickening is more evident in the central part of the Eastern Mediterranean, from Crete towards east and south of Turkey, beneath the central Aegean in particular along the Turkish coast. Remarkable differences are observed south of Cyprus, where the Eratosthenes seamount shows a thinner crust than the Levantine basin in the three layers.

Shear-wave velocity maps are shown in Figure 6, again compared to the starting model. In Figure 6, we define “upper-mantle” the first layer below the Moho, which shows then constant velocity in the initial model. Significant differences are found between the right and left panels in Figure 6, though in some cases gross features in CRUST2.0+IASP91 also appear in the final model (for example hard sediment and upper crust maps). Sediments show faster shear velocities with respect to the initial model, specifically in the Aegean region, southwest Turkey and central basin. However anomalously slow velocities are obtained in the crustal layers as well as in the upper-mantle. In particular, low shear wave velocities are imaged in the mid-crustal layer in the central basin, in the lower crust in east-north east of Cyprus, and in most of the basin in the upper-mantle layer. In the northern Aegean region, an important characteristic to emphasize is the high (3.8-3.9 km/s) S-velocity of the upper and middle crust layers. These velocities, which are significantly higher than the ones in the initial model, decrease and become more localized from the upper crust down to the lower crust.

In Turkey crustal shear velocities vary roughly in the range 3.4-3.6 km/s in the first two layers for the whole region but show significant variation in the lower crust. In fact shear wave velocities in western Turkey are ~3.6-3.7 km/s but they increase to 3.9 km/s in central Turkey to reach ~4 km/s in the Eastern Anatolian Fault and southwards.

From the Eratosthenes seamount to the Jordan coast a general increasing of the shear velocity is observed in the three crustal layers. Beneath Cyprus, mostly the northwestern part, the velocity has roughly the same value (~3.5 km/s) in the upper and middle layer, but becomes significantly higher in the lower crust.

In the upper-mantle, a clear strip of low shear wave velocities runs from west (Tyrrhenian sea in Italy) to east (Cyprus), and from north (northern Aegean and the North Anatolian Fault) southward (Crete and the Libyan sea, Dead Sea Fault and Egypt), with well defined regions of high velocities such as western Greece, south-western Turkey, Arabia, the Mediterranean basin, north Africa and the Ionian sea. Away from the subduction zones, we also find anomalously low velocities in the upper-mantle beneath central Turkey, as also shown in previous studies (Marone *et al.*, 2003; Meier *et al.*, 2004; Gok *et al.*, 2006). Our results in light of these previous studies suggest a thinned lithosphere, as well-documented for Eastern Turkey, is present in this region.

DISCUSSION

Figure 7 shows plots of sediment and crustal thickness, where important features are revealed. The sediment thickness (Figure 7, top) increases beneath the central part of the Eastern Mediterranean basin, Crete island, Cyprian arc and Aegean region, including southern Greece, making Figure 7 (top) appear more like the intermediate period group velocities in Figure 3a (central panel). A significant amount of sediments are found south of Crete, increasing from west to east and being deeper than 10 km in the Libyan Sea and eastward.

A shallower crust (Figure 7, bottom) is derived in the Ionian sea, southern Italy and the central part of the Eastern Mediterranean basin. The crustal thickness (Figure 7, bottom) deepens in the south Ionian basin and Cyprus, making the map more like the long period group velocities shown in Figure 3a (bottom panel). Crustal thickness (Figure 7, bottom) generally decreases from north to south and from east to west.

In the following text, we systematically describe Figure 7 comparing the results in specific areas to those from previous studies to see how they differ.

Greece. Sedimentary layer in Greece (Figure 7, top) is generally very shallow, although it deepens beneath the Peloponnesus, reaching 6-8 km thickness. Beneath Greece, crustal thicknesses range from 30 km in Peloponnesus to 40 km and more in the Hellenides and continental Greece (Figure 7, bottom). Similarly Marone *et al.* (2003) found a very deep Moho beneath continental Greece and the Peloponnesus (> 40 km). In general crustal thickness pattern plotted in Figure 7 (bottom) results very similar to that from Marone *et al.* (2003).

Aegean. In northern and central Aegean sediment thickness is in the range 3-5 km, and the

deeper values are found in the west-central Aegean sea. Moving southward a progressive increase in the sedimentary cover is revealed and depths of maximum 10 km are mapped at north of Crete. In the Aegean Sea, the crust thins from north southward. We find crustal thickness of 20-25 km in the southern, central-western Aegean, whereas it reaches 32 km in the northern and south-eastern Aegean. These values are in good agreement with previous work by van der Meijde *et al.* (2003). A map of crustal thickness in the Aegean, recently obtained from the inversion of gravity data (Tirel *et al.*, 2004), also shows a pronounced NE-SW trending of crustal thinning in the northern Aegean probably due to the numerous basins present there. Similarly, Karagianni *et al.* (2005), by inverting surface waves, found a crust of 20-22 km in central and southern Aegean, 28-30 km in the inner Aegean, 40–46 km under the Hellenides in western Greece, and 30–34 km in the eastern continental Greece.

Crete. Beneath the Cretan sea and Crete island the crustal thicknesses deepen from 26 km in south-west of Crete to 39 km in central-northern Crete. This trend has been previously observed by other authors (Li *et al.*, 2003; van der Meijde *et al.*, 2003), although the lower resolution of the surface waves does not allow us to evidence the details at local scale as in the cited papers. Marone *et al.* (2003) found crustal thickness in the range of 25-32 km beneath Crete island. In central and eastern Crete, gravity data inversion (Makris & Yegorova, 2005) revealed Moho depths in the ranges 32-34 km and 24-26 km respectively, values that are in good agreement with those in Figure 7. From Figure 7 (bottom), a sediment layer ~ 8 km is obtained in Crete, but no difference is found in central with respect to western Crete as found in other studies (Endrun *et al.*). Makris & Yegorova (2005) obtained

sediments thick 10-14 km and a Moho depth of 18-24 km outside Crete. In the same study, they found that Cretan sea has a relatively thinner continental crust (15-20 km depth) including 3-4 km of sediments.

Cyprus and surroundings. In Figure 7 (bottom) the nature of the crust varies along the island with respect to the south and from the Levantine basin to the Eratosthenes seamount. We find a thicker crust (30-34 km) beneath Cyprus and in the Levantine basin with respect to the 22-24 km in the Eratosthenes seamount, sediment thickness of ~10 (and beyond) and ~6 km is mapped in the two areas respectively, according to the top plot in Figure 7. Indeed the tomographic inversion of local data (Koulakov & Sobolev, 2005) reveals a thicker crust of ~33 km beneath Cyprus and ~27 km in the Eratosthenes seamount. Gravity data show a higher Bouguer anomaly in Cyprus with respect to the Eratosthenes seamount (Khair & Tsokas, 1999), and also seismic and magnetic data (Makris *et al.*, 1983; Ben Avraham *et al.*, 2002) confirm the variation of the crust type in this region of the Mediterranean. Our results significantly differ from Marone's *et al.* (2003) study, in a N-S swath extending across the Eastern Mediterranean between Cyprus and Crete, where they find a band of thick crust (> 30 km). According to Figure 7 (bottom), the crust deepens from Cyprus eastward, assuming values from 28-30 km beneath the coast to 38-40 km beneath the continent.

The issue about the continental or oceanic nature of the crust beneath the Eratosthenes seamount and the Levantine basin is still a matter of discussion. From results in Figure 7 we conclude that the crust is continental-like crust, as many authors suggest (Ben-Avraham *et al.*, 2002 and

reference therein) and whose thickness varies in the range 22-26 km. The existence of continental-type crustal blocks in the eastern Mediterranean basin is due, as suggested by many authors, to the rifting from the African continental crust (Ben-Avraham *et al.*, 2002 and reference therein).

Turkey and the Arabian Plate. The sedimentary cover beneath most of Turkey and Arabia is very shallow. In the Dead Sea Fault area a sedimentary layer of 3-5 km is observed. The deepest crust (Figure 7, bottom) is observed in Turkey and in the Dead Sea Fault zone. In western Turkey the Moho discontinuity is thinner beneath the west coast but thicker inland where ~50 km depth is observed; the crustal thickness becomes shallower in the Eastern Anatolian Fault and southwards. Our model significantly differ from the one in Marone *et al.* (2003), because our deeper Moho (sediment + crustal thicknesses) (> 40 km) in Turkey is shallower (30-40 km) in their study.

Figure 8 illustrates three profiles along which the estimated shear-wave velocities are projected using the same color scale used by Makris & Yegorova (2005). Depths in Figure 8 are comparable to the sum of the two maps (sediment and crustal thickness) in Figure 7. The cross-section A-A' has a SW-NE direction from north Africa to western Turkey and is comparable with the PR4 profile in Makris & Yegorova (2005). Beneath the Libyan Sea towards Crete slow velocities are found and corresponding crustal thicknesses vary in the range of 28-32 km, reaching a minimum in the Libyan Sea. The relatively slow velocities in the uppermost mantle extend from the Libyan Sea to the Aegean as also found by Meier *et al.* (2004). In contrast, high shear-wave velocities characterize northern Africa and western Turkey. Makris & Yegorova (2005) find the thinning of the sedimentary cover

from ~14 km in southern Crete to a few kilometers at ~60 km north of the African coast, due to the subduction of the cold oceanic lithosphere beneath the Aegean. This behavior is also observed in A-A' profile (Figure 8) from the Libyan Sea to the Aegean. The profile B-B' runs S-N from northern Egypt to Turkey through Cyprus. From south northward, crustal shear-wave velocities are low, in particular beneath northern part of Cyprus. High upper -mantle shear velocities are only obtained in the Eastern Mediterranean basin south of Cyprian arc. The profile C-C' runs from the Peloponnesus to Turkey through the Aegean Sea, showing slow upper-mantle shear wave velocities in the back of the Cretan and Cyprian arcs and fast upper-mantle in the back of the notch of the subduction zone (see Figure 1).

It is evident from Figure 6 and Figure 8 that slower velocities are displayed in the upper-mantle almost everywhere in the Eastern Mediterranean. The anomalously low velocities found in the upper-mantle in central Turkey (B-B' and C-C' profiles) are in agreement with results by Meier *et al.* (2004). In the uppermost mantle the low velocities along and in back of the subduction zones in Crete and Cyprus might be an indication of serpentinized mantle, as suggested also in other subduction zones (Hyndman & Peacock, 2003 and references therein). This probably relates to a hydrous or hydrothermal alteration as suggested in other subduction zones, where small percentage of serpentine in the crust would produce water in the mantle by the subducting crust (Hyndman & Peacock, 2003). The physical properties of the forearc mantle are affected by the presence of hydrous minerals as serpentine, which, if present, can decrease the seismic velocity (Hyndman & Peacock, 2003). The non purely oceanic nature of the crust in this area suggest that the composition of the upper-mantle is non basaltic which would have implied higher seismic velocities if either peridotite or eclogite were

predominant in the mineralogy (Kearey & Vine, 2004). We speculate that the uppermost mantle should be composed of partially serpentinized peridotite, with a certain amount of serpentine due to the fact that in some regions the observed S-wave velocities are around or below 4.3 km/s. This hypothesis is also supported by the low velocities associated with the lower crust in the same region since the seismic properties of the uppermost mantle are related to the type of the overlying lower crust. For a typical lower lithosphere in which seismic velocity increases with depth, shear-wave velocities characterizing the upper-mantle are expected to be faster than those imaged in Figure 6. Beneath the lithosphere roughly down to ~150 km depth, when melt or partial melting occur there the asthenosphere is present and seismic velocities are lower with respect to the uppermost mantle velocities. Partial melting in the upper mantle could explain the high heat flow observed in the Eastern Mediterranean, where sedimentation plays an important role (Ben-Avraham, *et al.*, 2002 and references therein; Kearey & Vine, 2004). Although different processes such as partial melting, water content, compositional or phase change, high temperature, can lower the seismic velocity (as in the Hellenic-Cyprian trench), either serpentinization or partial melting could be favorite candidates to explain the observed S-wave velocities.

In Figure 9 the Moho depths (sum of sediment and crustal thickness) obtained in this study are compared to those derived from other studies, including the error bars when available (bottom plot), for the locations shown in the map at the top panel of the same figure. In general, a deeper Moho is found here with respect to other studies. Many measurements are close or within ± 5 km although a certain number of discrepancies is observed. We ascribe most of the discrepancies to the presence of a

significant sedimentary layer in these sites. For instance, using the receiver function method, van der Meijde *et al.* (2003) find a crustal thickness of 43 km beneath ITHO (37.18°N-21.93°E) compared to 36 km in this study (Figure 7, bottom). That study showed a poor fit for the ITHO receiver function modeling in terms of both amplitude and timing of the different arrivals (Figure 6 of van der Meijde *et al.*, 2003) and they note the discrepancy with previous studies although they don't explain it. Very thick sediments and slow crustal velocities, found from Crete to Cyprus, should be considered in extracting the Moho depth.

In defining the fit goodness of Figure 9, it should be kept in mind the main difference between surface wave and receiver function studies. Surface waves resolve the absolute shear wave velocity at depths deepening with longer periods and the receiver functions constrain small scale relative shear wave velocity. In both cases there is a problem of non-uniqueness caused by a trade-off between depth and velocity, and an a-priori velocity model is needed in the inverse problem. Following Pasyanos & Walter (2002), we believe that uncertainties of ± 5 km in crustal thickness and ± 0.2 km/s in shear wave velocity are reasonable estimates and that the average crustal velocity is better constrained than the velocity in any individual layer. In addition, surface waves are sensitive to average shear wave velocities so they do not resolve sharp discontinuities but smoother velocity structure. Although the joint inversion of teleseismic receiver functions and regional or teleseismic dispersion curves can better image the earth structure than using each dataset separately, we believe that the results from our study are reliable because of the large number of data used in the tomographic inversion.

CONCLUSIONS

In this paper, maps of the shear-wave velocity, sediment thickness, and Moho depth are derived from the analysis of the dispersive characteristics of surface waves. Keeping in mind that the inversion of dispersion curves is affected by the intrinsic depth-velocity trade-off and that an initial model is still needed to start the iterative processing we believe that results from this study are reliable and significant due to large amount of collected data. We have found several important features in the crust and upper-mantle beneath the eastern Mediterranean region. A significant contrast between the oceanic and continental crust is well delineated at the boundary of the Hellenic subduction zone and the Ionian Sea where thin oceanic crust is mapped. The difference in the derived Moho depth coincides with the distinct bathymetry in the two areas. The central part of the eastern Mediterranean basin shows intermediate crustal thicknesses (16-26 km). In the same area, including the Cretan and Libyan seas and perpendicular to the Hellenic trench, a thick sedimentary blanket is present and reaches 14 km in the middle of the basin. In the Aegean region the crustal thickness generally decreases from north to south, remaining deeper to the east along the Turkish coastline and beneath the Peloponnesus to the west. A Moho discontinuity deeper than 30 km up to and over 50 km is obtained in western Greece, Turkey, North Africa and Arabia.

We have observed an inverse correlation between sediment and crustal thickness, previously only observed in extensional tectonic regimes (Ritzmann *et al.*, 2006) where thinned crust acquires correspondingly thicker sedimentary column. Our result suggests that in convergence regimes, as

subduction proceeds the topographically-high regions with thick crust shed their sediments, while the regions where thin crust remains accumulate them.

The presence of high crustal velocities in the north-central Aegean and relatively thick crust are associated with the presence of metamorphic core complex as extensively discussed in Zhu *et al.* (2006). In general, the upper mantle shear wave velocities are slower than the ones in corresponding layers of the initial model. Reduced shear- wave velocities are displayed in the upper-mantle almost everywhere in the study area, except at the southern part of the Ionian Sea, some portions in North Africa, southern Italy and western Greece. Finally, in the Eastern Mediterranean basin the presence of partially molten material as well as the presence of serpentinite could explain the observation of slow seismic velocities.

ACKNOWLEDGMENTS

We would like to thank M. Ritzwoller and A. Levshin for providing their group velocity measurements, S. Hazler and M. Benoit for making some of the dispersion curve measurements included in this study, C. Ammon for providing the PGSWMFA code to measure the dispersion, and R. Herrmann for making his codes available on-line. We also wish to thank editor G. R. Keller and two anonymous reviewers for their helpful comments.

We used Generic Mapping Tools (GMT) to produce the figures. This work has been partly done while F. Di Luccio was Visiting Associate at Seismological Laboratory of the California Institute of Technology, Pasadena, CA. This work was performed under the auspices of the U.S. Department of

Energy by the University of California, Lawrence Livermore National Laboratory under contract W-7405-ENG-48. This is LLNL contribution UCRL-JRNL-222138.

References

- Aksu, A. E., J. Hall and C. Yaltirak, 2005. Miocene to recent tectonic evolution of the eastern Mediterranean: New pieces of the old Mediterranean puzzle, *Marine Geology*, 221, 1-13.
- Al-Damegh, K., E. Sandvol, and M. Barazangi, 2005. Crustal structure of the Arabian plate: New constraints from the analysis of teleseismic receiver functions, *Earth Planet. Sci. Lett.*, 231, 177-196.
- Bassin, C., G. Laske and G. Masters, 2000. The current limits of resolution for surface wave tomography in North America, *EOS Trans AGU*, 81, F897.
- Ben-Avraham, Z., A. Ginzburg, J. Makris and L. Eppelbaum, 2002. Crustal structure of the Levant Basin, eastern Mediterranean, *Tectonophysics*, 346, 23-43.
- Endrun, B., T. Meier, M. Bischoff and H.-P. Harjes, 2004. Lithospheric structure in the area of Crete constrained by receiver functions and dispersion analysis of Rayleigh phase velocities, *Geophys. J. Int.*, 158, 592-608.
- Gok, R., M.E. Pasyanos, and E. Zor, 2006. Lithospheric structure of the continent-continent collision zone: Eastern Turkey, *Geophys. J. Int.*, in press.
- Herrmann, R.B., 1973. Some aspects of bandpass filtering of surface waves, *Bull. Seism. Soc. Amer.*, 63, 663-671.
- Herrmann, R. B., and C. J. Ammon, 2002. Computer programs in seismology - surface waves, receiver

functions and crustal structure, Saint Louis University,

<http://www.eas.slu.edu/People/RBHerrmann/ComputerPrograms.html>.

Hofstetter, A., and G. Bock, 2004. Shear-wave velocity structure of the Sinai subplate from receiver function analysis, *Geophys. J. Int.*, 158, 67-84, doi:10.1111/j.1365-246X.2004.02218.x.

Hyndman, R.D., and S.M. Peacock, 2003. Serpentinization of the forearc mantle, *Earth Planet. Sci. Lett.*, 212, 417-432.

Karagianni, E. E., C. B. Papazachos, D. G. Panagiotopoulos, P. Suhadolc, A. Vuan and G. F. Panza, 2005. Shear velocity structure in the Aegean area obtained by inversion of Rayleigh waves, *Geophys. J. Int.*, 160, 127-143.

Kearey, P., and F.J. Vine,, 2004. *Global Tectonics*, 2nd ed., 19-28, published by Blackwell Science.

Kennett, B. L. N., and E. R. Engdahl, 1991. Traveltimes for global earthquake location and phase identification, *Geophys. J. Int.*, 105, 429-465.

Khair, K., and G. N. Tsokas, 1999. Nature of the Levantine (eastern Mediterranean) crust from multiple-source Werner deconvolution of Bouguer gravity anomalies, *J. Geophys. Res.*, 104(B11), 25,469-25,478.

Koulakov, I., and S. V. Sobolev, 2005. Moho depth and three-dimensional P and S structure of the crust and uppermost mantle in the Eastern Mediterranean and Middle East derived from tomographic inversion of local ISC data, *Geophys. J. Int.*, doi: 10.1111/j.1365-246X.2005.02791.x.

- Li, X., G. Bock, A. Vafidis, R. Kind, H. P. Harjes, W. Hanka, K. Wylegalla, M. van der Meijde and X. Yuan, 2003. Receiver function study of the Hellenic subduction zone: imaging crustal thickness variations and the oceanic Moho of the descending African lithosphere, *Geophys. J. Int.*, 155, 733-748.
- Makris, J., 1985. Geophysics and geodynamic implications for the evolution of the Hellenides, in *Geological Evolution of the Mediterranean Basin*, 231-248, Eds. Stanley, D. & Wezel, F., Springer, Berlin.
- Makris, J., Z. Ben-Avraham, A. Behle, A. Ginzburg, A. Giese, L. Steinmetz, R. B. Whitmarsh, and S. Eleftheriou, 1983. Seismic refraction profiles between Cyprus and Israel and their interpretation, *Geophys. J. R. Astron. Soc.*, 75, 575-591.
- Makris, J., and T. Yegorova, 2005. A 3-D density-velocity model between the Cretan Sea and Libya, *Tectonophysics*, doi:10.1016/j.tecto.2005.11.03.
- Marone, F., M. van der Meijde, S. van der Lee and D. Giardini, 2003. Joint inversion of local, regional and teleseismic data for crustal thickness in the Eurasia-Africa plate boundary, *Geophys. J. Int.*, 154, 499-514.
- McClusky, S., S. Balassanian, A. Barka, C. Demir, S. Ergintav, I. Georgiev, O. Gurkan, M. Hamburger, K. Hurst, H. Kahle, K. Kastens, G. Kekelidze, R. King, V. Kotzev, O. Lenk, S. Mahmoud, A. Mishin, M. Nadariva, A. Ouzounis, D. Paradissis, Y. Peter, M. Prilepin, R. Reilinger, I. Sanli, H. Seeger, A. Tealeb, M. N. Toksöz, and C. Veis, 2000. Global Positioning System constraints on plate kinematics and dynamics in the eastern Mediterranean and

Caucasus, *J. Geophys. Res.*, 105, 5695-5719.

McClusky, S., R. Reilinger, S. Mahmoud, D. Ben Sari, and A. Tealeb, 2003. GPS constraints on Africa (Nubia) and Arabia plate motions, *Geophys. J. Int.*, 155, 126-138.

Meier, T., K. Dietrich, B. Stöckhert and H. -P. Harjer, 2004. One-dimensional models of shear wave velocities for the eastern Mediterranean obtained from the inversion of Rayleigh wave phase velocities and tectonic implications, *Geophys. J. Int.*, 156, 45-58, doi: 10.1111/j.1365-246X.2004.02121.x.

Mohsen, A., R. Hofstetter, G. Bock, R. Kind, M. Weber, K. Wylegalla, G. Rumpker, and the DESERT Group, 2005. *Geophys. J. Int.*, 160, 948-960, doi:10.1111/j.1365-246X.2005.02534.x.

Netzeband, G. L., K. Gohl, C. P. Hubscher, Z. Ben-Avraham, G. A. Dehghani, D. Gajewski, and P. Liersch, 2006. The Levantine Basin-crustal structure and origin. *Tectonophysics*, 418, 167-188, doi:10.1016/j.tecto.2006.01.001.

Pasyanos, M.E., 2005. A variable resolution surface wave dispersion study of Eurasia, North Africa, and surrounding regions, *J. Geophys. Res.*, 110, B12301, doi:10.1029/2005JB003749.

Pasyanos, M. E., and Walter, 2002. Crust and upper-mantle structure of North Africa, Europe and the Middle East from inversion of surface waves, *Geophys. J. Int.*, 149, 463–481.

Ritzmann, O., N. Maercklin, J.I. Faleide, H. Bungum, W.D. Mooney, and S.T. Detweiler, 2006. A 3D geophysical model for the crust in the greater Barents Sea region: Database compilation, model construction and basement characterization, submitted to *Geophys. J. Int.*

- Tirel, C., F. Gueydan, C. Tiberi, and J. P. Brun, 2004. Aegean crustal thickness inferred from gravity inversion. Geodynamical implications, *Earth Planet. Sci. Lett.*, 228, 267-280.
- van der Meijde, M., S. van der Lee and D. Giardini, 2003. Crustal structure beneath broad-band seismic stations in the Mediterranean region, *Geophys. J. Int.*, 152, 729-739.
- Wdowinski, S., Z. Ben-Avraham, R. Arvidsson and G. Ekström, 2006. Seismotectonics of the Cyprian Arc, *Geophys. J. Int.*, 164, 176-181, doi: 10.1111/j.1365-246X.2005.02737.x
- Weber, M.; K. Abu-Ayyash, A. Abueladas, A. Agnon, H. Al-Amoush, A. Babeyko, Y. Bartov, M. Baumann, Z. Ben-Avraham, G. Bock, J. Bribach, R. El-Kelani, A. Förster, H. J. Förster, U. Frieslander, Z. Garfunkel, S. Grunewald, H. J. Götze, V. Haak, C. Haberland, M. Hassouneh, S. Helwig, A. Hofstetter, K. H. Jäckel, D. Kesten, R. Kind, N. Maercklin, J. Mechie, A. Mohsen, F. M. Neubauer, R. Oberhänsli, I. Qabbani, O. Ritter, G. Rumpker, M. Rybakov, T. Ryberg, F. Scherbaum, J. Schmidt, A. Schulze, S. Sobolev, M. Stiller, H. Thoss, U. Weckmann, K. Wylegalla, 2004. The crustal structure of the Dead Sea Transform, *Geophys. J. Int.*, 156, 655-681.
- Zor, E., E. Sandvol, C. Gurbuz, N. Turkelli and D. Seber, 2003. The crustal structure of the East Anatolian plateau (Turkey) from receiver functions, *Geophys. Res. Lett.*, 30, doi:10.1029/2003GL018192.
- Zhu, L., B. J. Mitchell, N. Akyol, I. Cemen, and K. Kekovali, 2006. Crustal thickness variations in the Aegean region and implications for the extension of continental crust, *J. Geophys. Res.*, 111, doi:10.1029/2005JB003770.

FIGURE CAPTIONS

Figure 1. Simplified tectonic and topographic map of the Eastern Mediterranean. The heavy gray arrows indicate the plate motions with respect to Eurasia, whereas the thinner black arrows show the main fault movements. Regional motions and relative rates are from McClusky *et al.* (2003). Red arrows in the northern Aegean sea and western Turkey indicate the NE-SW and N-S extension respectively. Last two decades of seismicity ($M > 4$), derived from the NEIC catalog, are also plotted. N.A.F. = North Anatolian Fault; E.A.F. = East Anatolian Fault; D. S. F. = Dead Sea Fault; MS = Marmara Sea; TS = Tyrrhenian Sea; CA = Calabrian Arc; ES = Eratosthenes Seamount; LB = Levantine Basin; HB = Herodotus Basin; PST = Pliny-Strabo Trench; FR = Florence Rise.

Figure 2. Maps of measured Rayleigh wave group velocity paths for the Eastern Mediterranean for 15 s, 30 s, and 50 s period. In each figure, blue lines indicate paths, yellow circles earthquakes, and red triangles seismic stations.

Figure 3a. Maps of Rayleigh wave group velocities determined by seismic tomography for 15 s, 30 s, and 50 s period. In each figure, red colors are slow and blue colors are fast.

Figure 3b. Maps of Rayleigh wave group velocity uncertainties corresponding to Figure 3a.

Figure 4. Fitting of the dispersion data to the predicted Rayleigh and Love wave group velocities (top panel). In the bottom panel (left) the obtained (dashed) shear-wave velocities versus depth are plotted with respect to the initial models (solid). Gray lines indicate the IASP91 model used as starting model and the output model (dashed lines). In order to show the differences between two sets of models at crustal depths, an enlargement of the left panel in the depth range 0-50 km is plotted at right.

Figure 5. A comparison of the sedimentary and crustal layers between the initial model (left panels) and the model obtained in this study (right panels). Layer separation is derived from CRUST2.0.

Figure 6. Shear-wave velocity maps derived from dispersion curve inversion (right panels) and compared to the starting model (left panels).

Figure 7. Sediment (top) and crustal (bottom) maps obtained in this study.

Figure 8. Cross-sections through different portions of the model. The top map provides the location of the cross-sections. The cross-sections are for a) SW-NW section across Crete, b) a S-N section across Cyprus, and c) a W-E cross-section across Greece and Western Turkey.

Figure 9. Moho depth derived in this study plotted versus the one obtained from other studies including the error bars when available. The dashed lines represent the ± 5 km interval.

A=Al-Damegh *et al.* (2005); H=Hofstetter & Bock (2004); L=Li *et al.* (2003); M=Mohsen *et al.* (2005); Ma=Makris (1985); T=Tirel *et al.* (2004); V=van der Meijde *et al.* (2003); Zh=Zhu *et al.* (2006); Z=Zor *et al.* (2003).

Figure 1

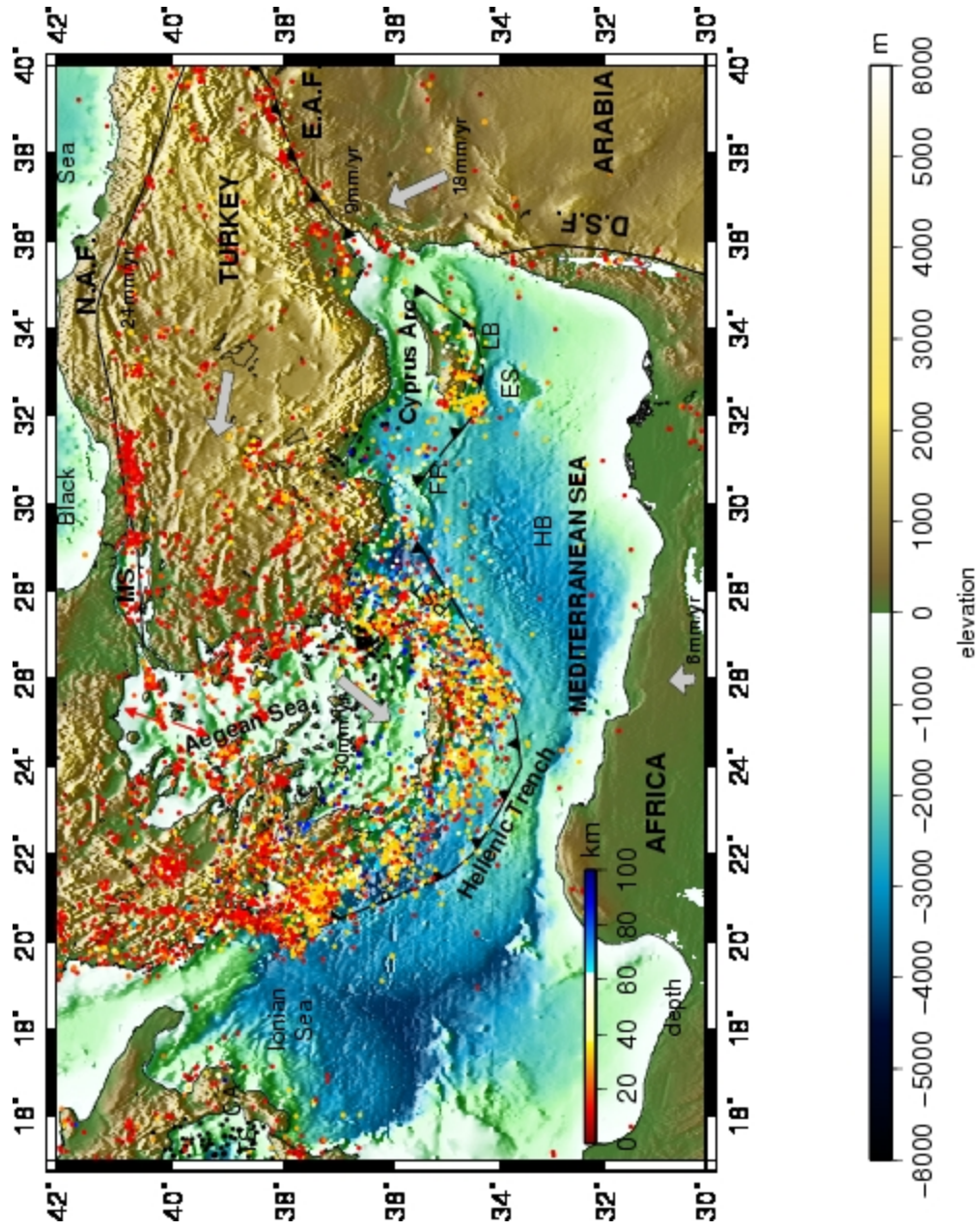


Figure 2

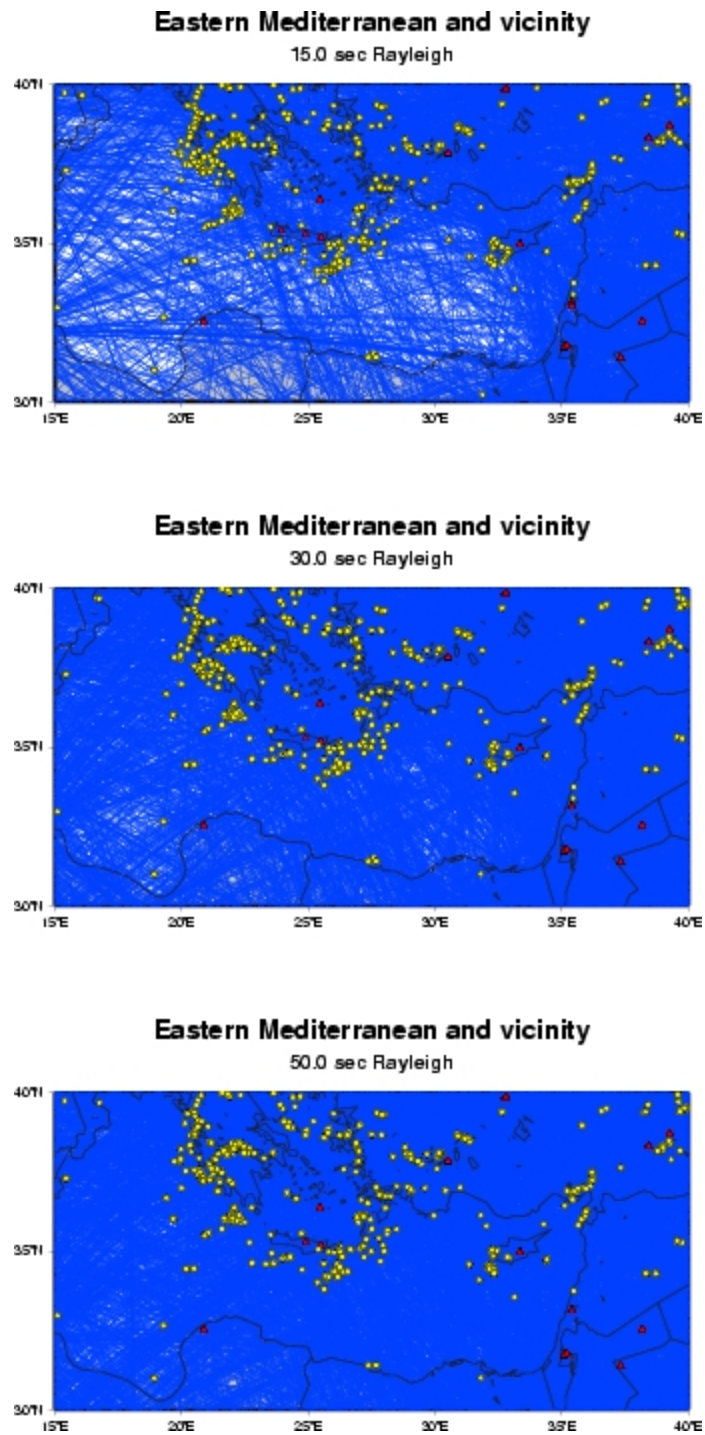


Figure 3a

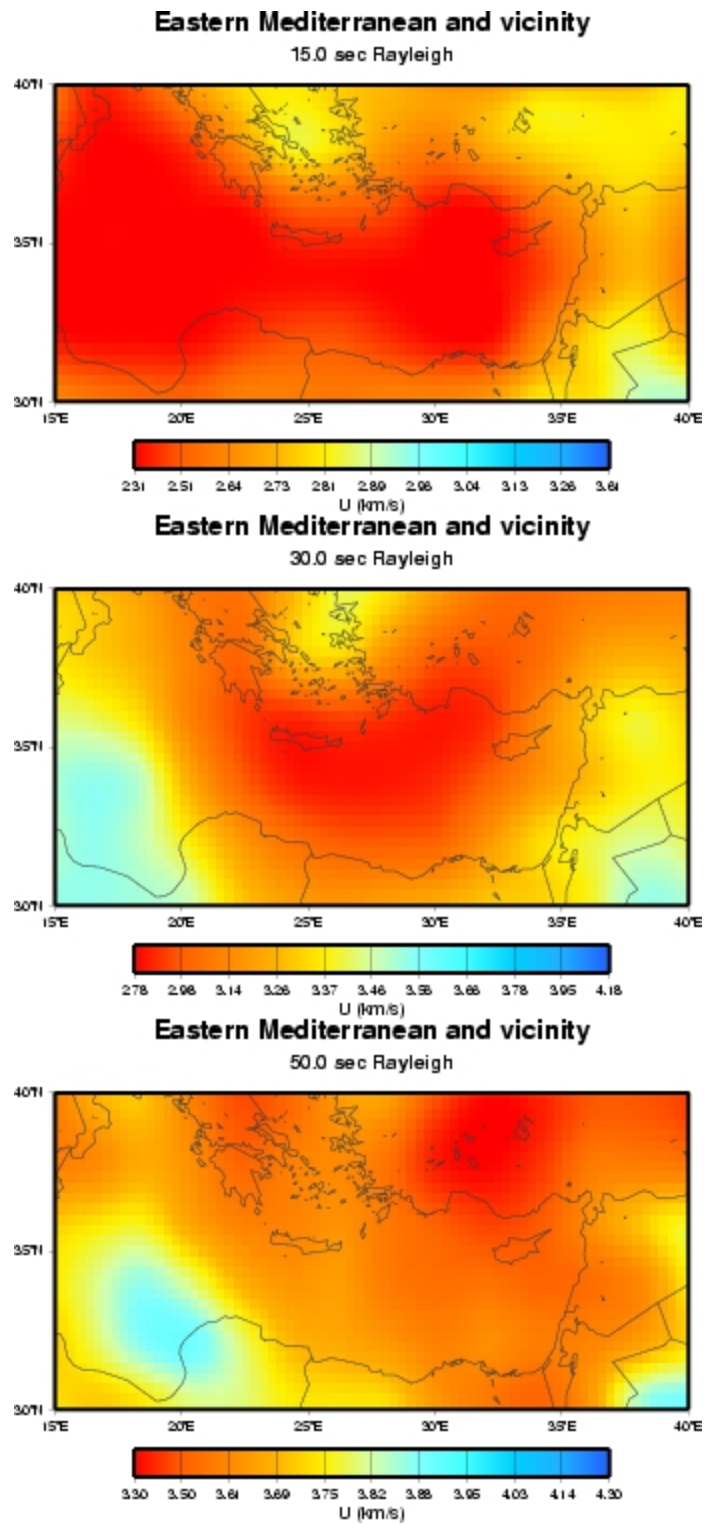


Figure 3b

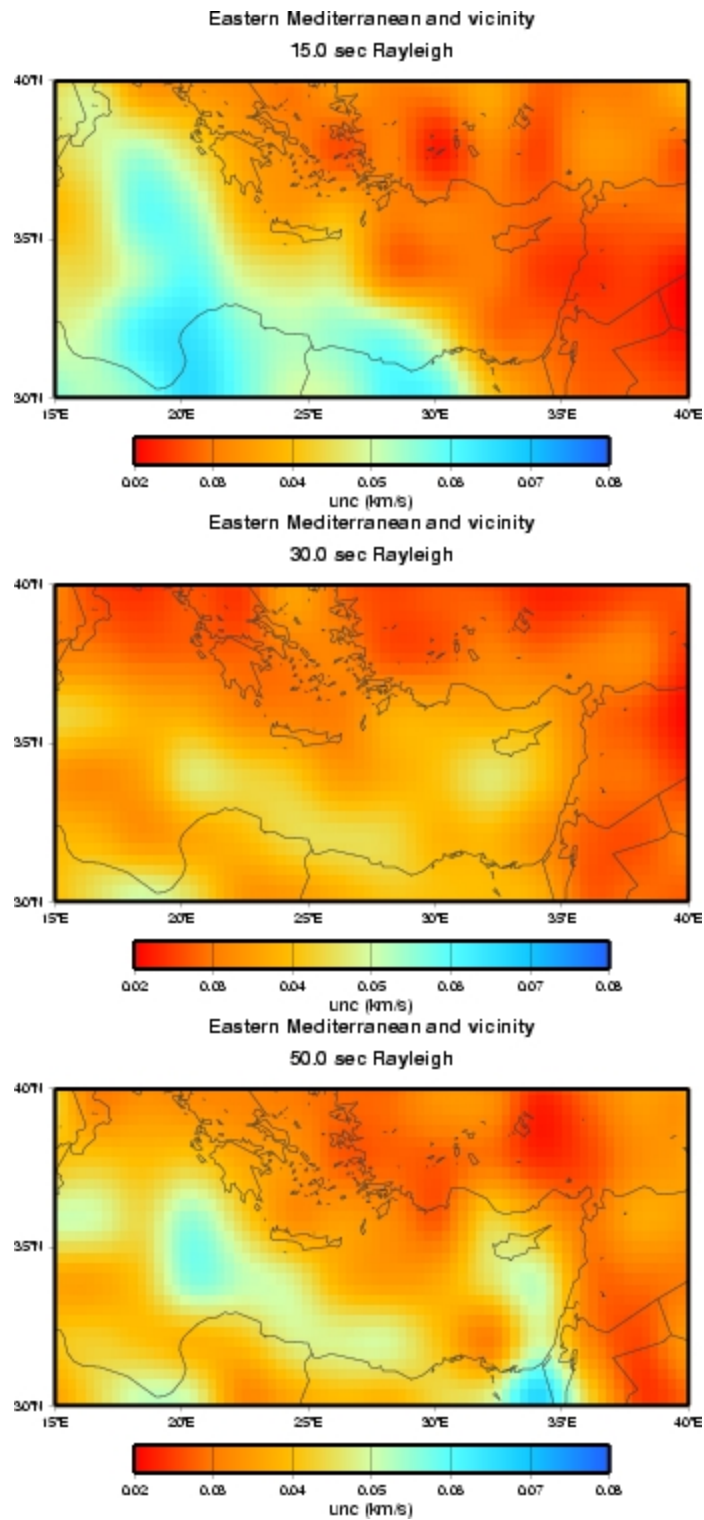


Figure 4

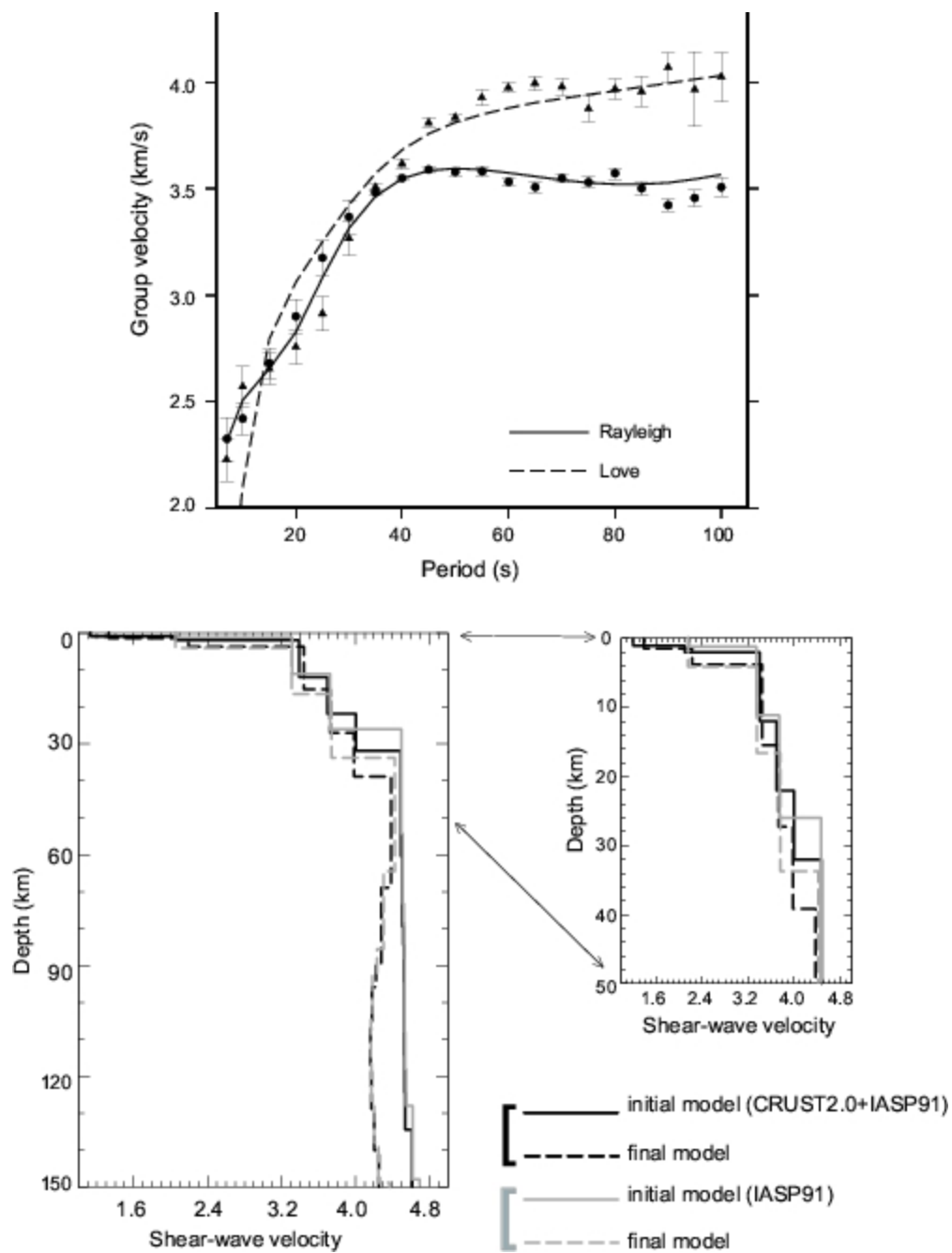


Figure 5

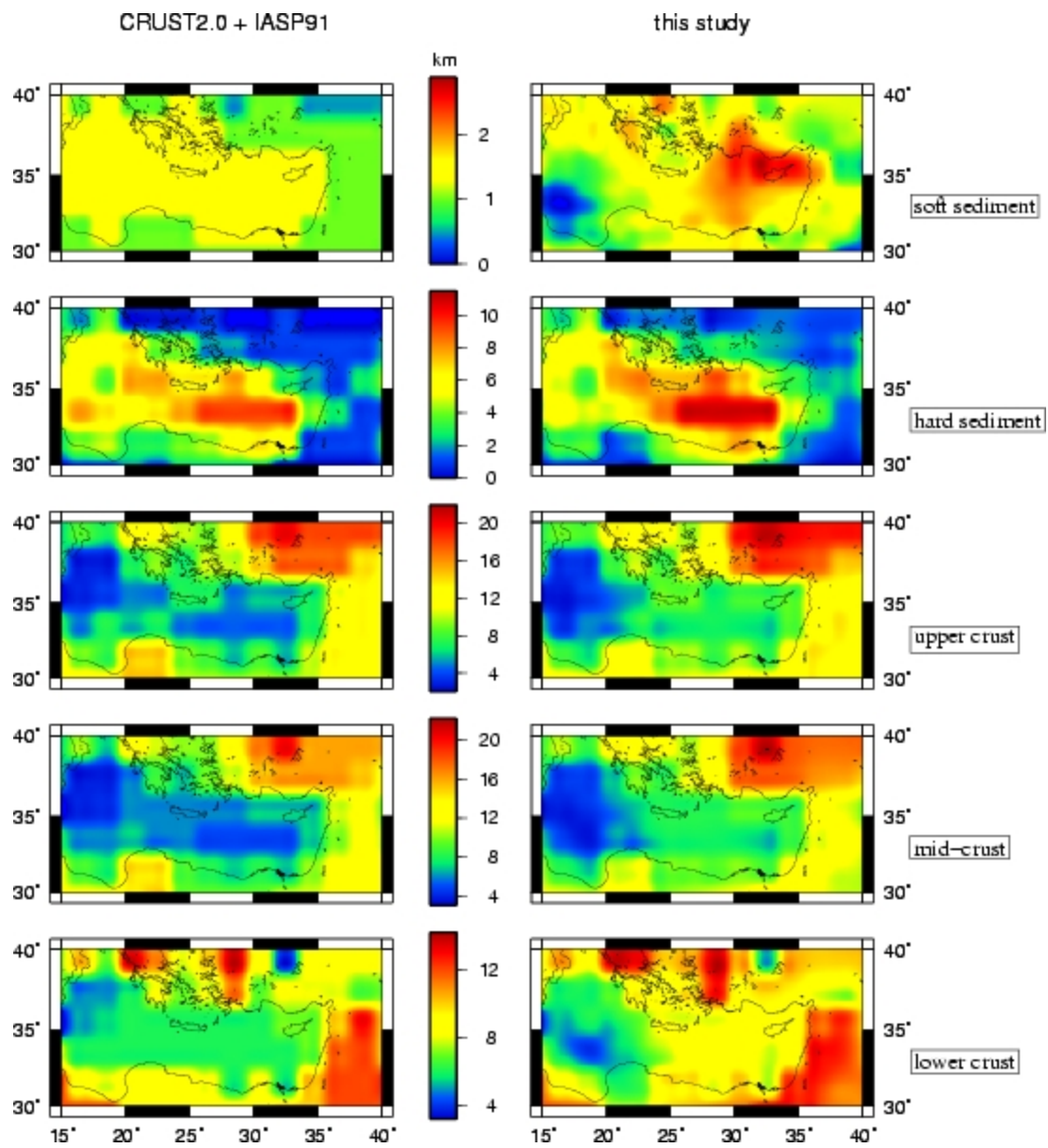


Figure 6

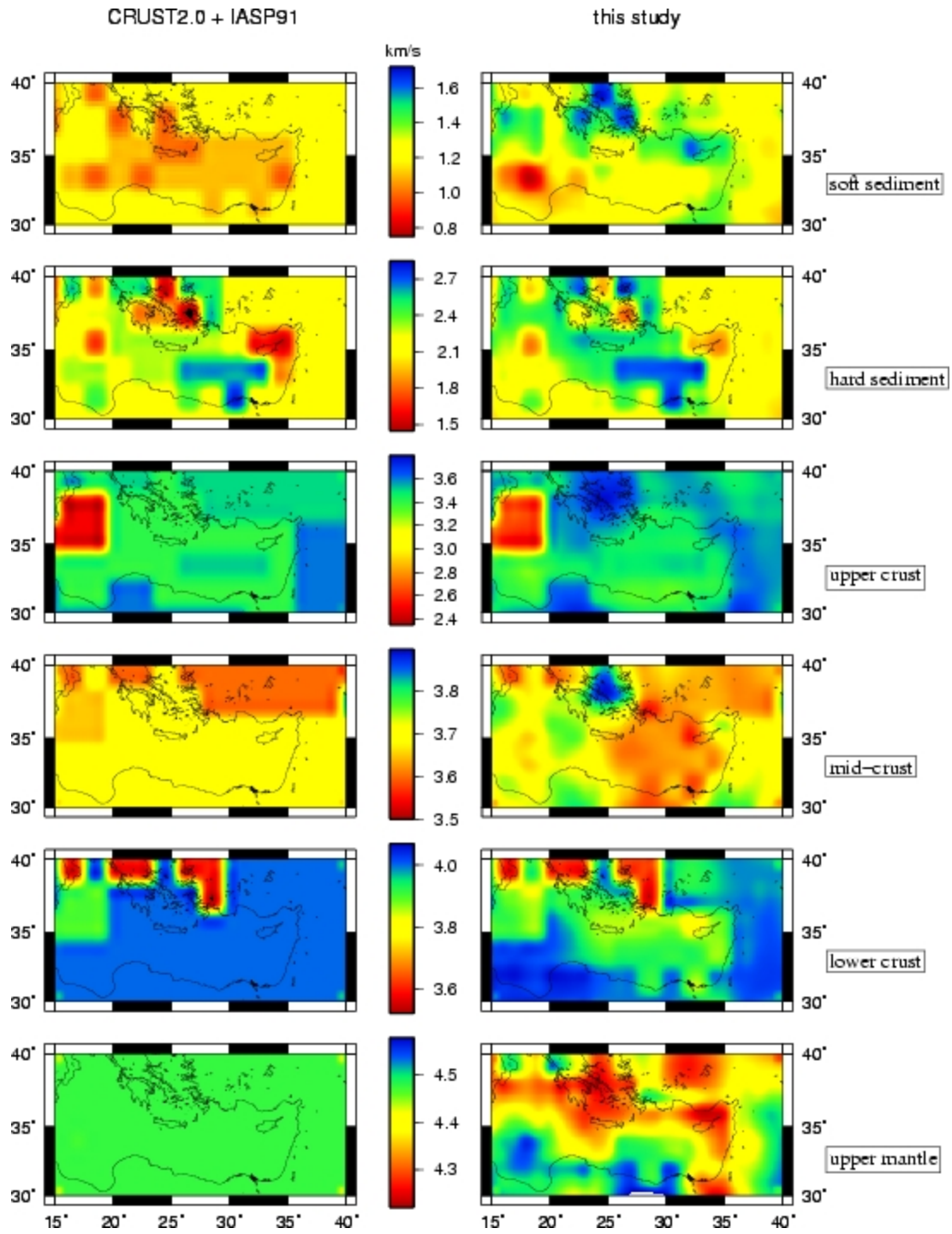


Figure 7

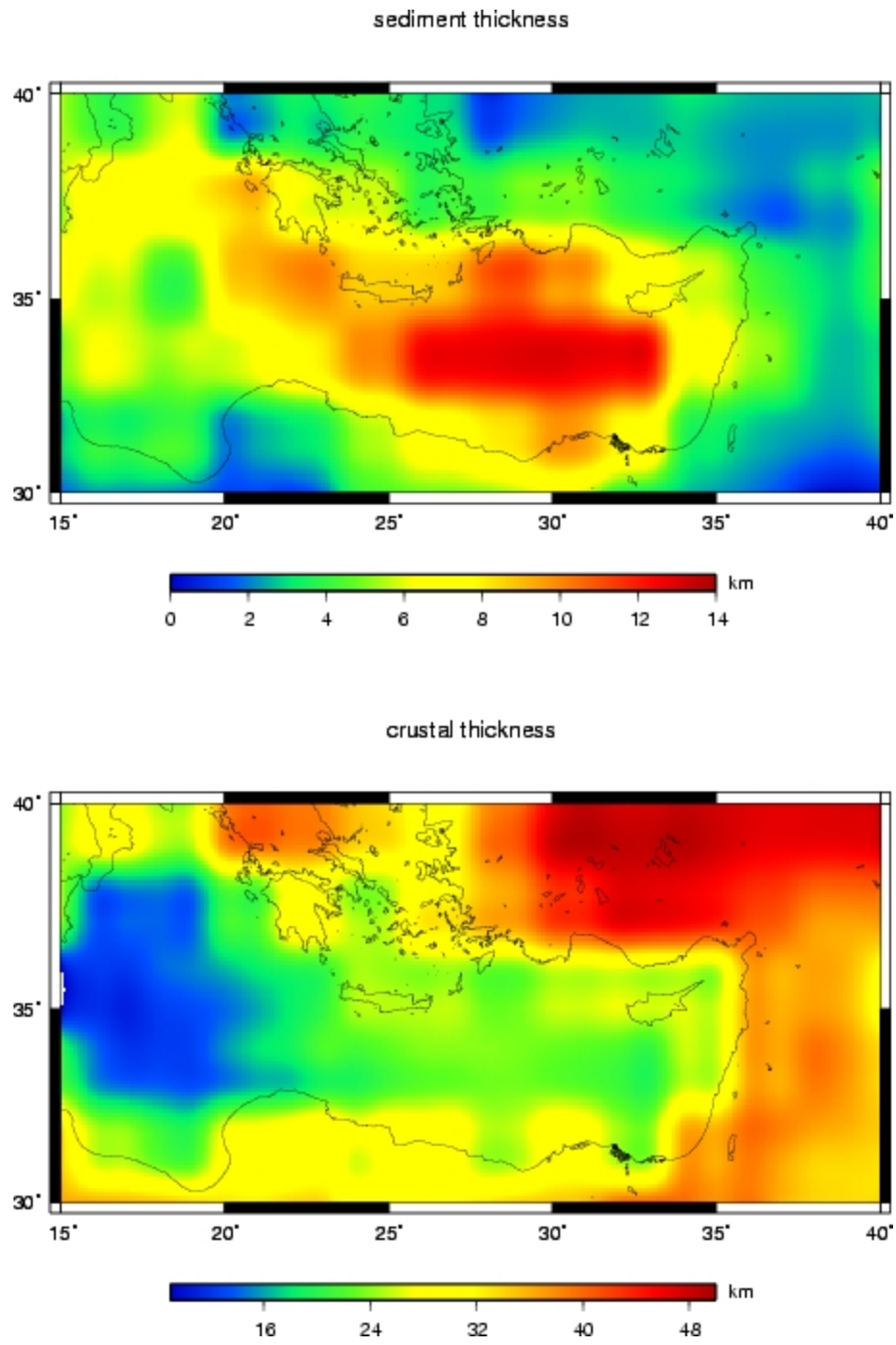


Figure 8

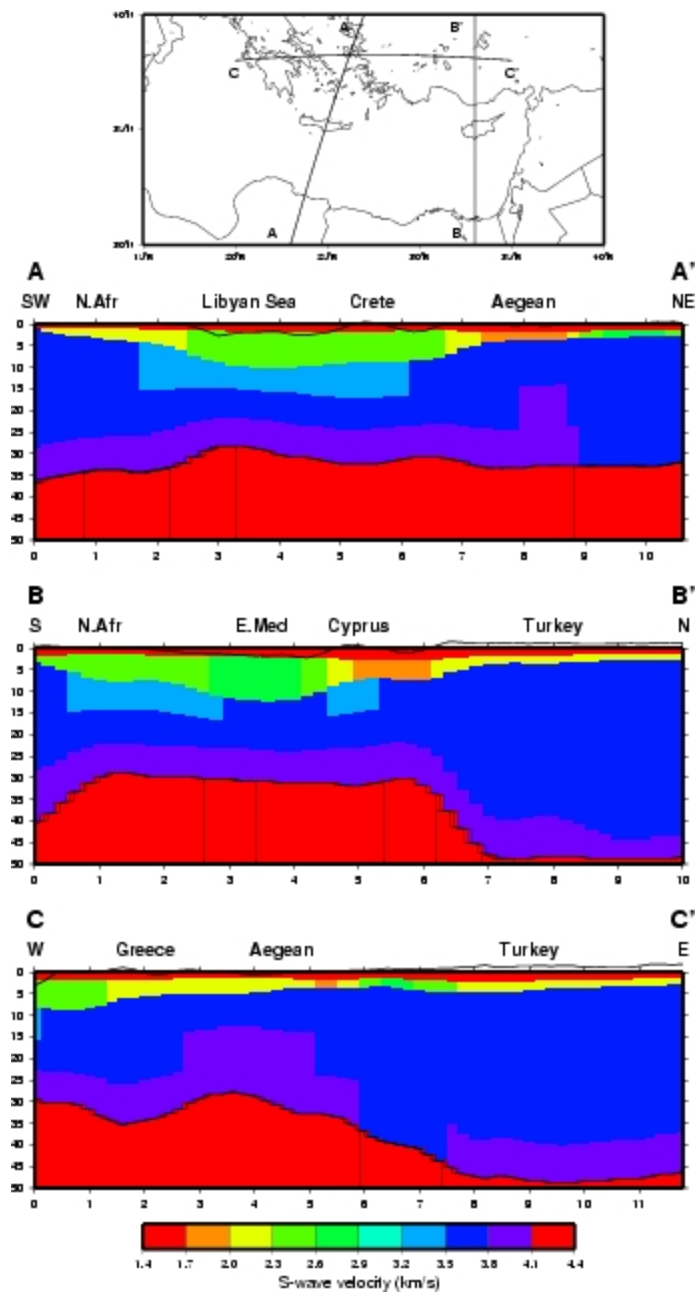


Figure 9

